Effects of thermal shocks on integrity of existing and newly-designed sealants for CCS applications

Li, Kai; Pluymakers, Anne M.H.

DOI
10.1016/j.ijggc.2024.104103

Publication date
2024

Document Version
Final published version

Published in
International Journal of Greenhouse Gas Control

International Journal of Greenhouse Gas Control 133 (2024) 104103

Contents lists available at ScienceDirect

International Journal of Greenhouse Gas Control

journal homepage: www.elsevier.com/locate/ijggc

Effects of thermal shocks on integrity of existing and newly-designed sealants for CCS applications

Kai Li *, Anne M.H. Pluymakers

Geoscience & Engineering Department, Delft University of Technology, the Netherlands

ARTICLE INFO

Keywords:
CCS
Well integrity
Sealants
Thermal shocks
Thermally-induced cracking

ABSTRACT

Sealants that can guarantee long-term wellbore sealing integrity are of great significance to the safe and sustainable storage of CO_2 in carbon capture and storage (CCS). In this study, we investigate how abrupt cyclic thermal shocks affect the integrity of four sealants of different compositions. These sealants include two reference OPC-based blends (S1 and S2), one newly-designed OPC-based blend that contains CO_2-sequestering additives (S3), and one calcium aluminate cement (CAC)-based blend designed for CCS applications (S4). We have measured the thermal properties of these samples, followed by quenching and flow-through experiments to apply strong cyclic thermal shocks on samples of the four sealants, where we heated the samples to 120 °C, and quenched them in, or flowed through water of 20 °C. Using X-ray tomography (32 μm/voxel) before and after the experiment showed that both S1, S2 (reference OPC-based) and S4 (CAC-based) broke after thermal-shocking experiments. Cracks and new voids developed in the samples. Post-treatment strength testing shows that thermal shocks reduce the unconfined compressive strength of these three sealants. This implies that these compositions may not be optimal materials for long-term wellbore sealing during CO_2 injection and storage afterward. For all these three sealant compositions, quenching resulted in a greater reduction in strength (by 53 % on average) than flow-through experiments (by 29 % on average). On the contrary, we have not observed any cracks after either quenching or flow-through experiments in S3 sealant (OPC with CO_2-sequestering additives). We attribute the intactness of this sealant after thermal shocks to its higher thermal diffusivity than the other three sealants. Heat transfers more rapidly in this sealant and the associated thermal stresses are mild and insufficient to cause any damage to its integrity, which makes this sealant a good candidate for wellbore sealing material that can effectively withstand strong thermal shocks encountered during CCS, though further studies are required.

1. Introduction

Carbon capture and storage (CCS), an technology to remove CO_2 from the atmosphere and store it in subsurface formations such as depleted oil and gas reservoirs or saline aquifers, has gained much attention in the last decades, as it contributes to fighting global climate change by reducing CO_2 emissions (Metz et al., 2005; Haszeldine, 2009; Selma et al., 2014; Budinis et al., 2018; Bui et al., 2018). The success of subsurface CO_2 storage depends on the permanent residence of CO_2 in the targeted reservoirs. However, during CCS, the periodic injection of pressurized cold CO_2 (Alnes et al., 2011; Eiken et al., 2011; Yoo et al., 2013; Samara et al., 2022) into warm reservoirs leads to cyclic temperature fluctuations. It is not clear what the exact magnitude, rate or frequency of these temperature fluctuations would be during operation of a CO_2 storage site, since it would be affected by operational parameters, and if the CO_2 is delivered continuously through a pipeline (c.f. the planned Portos project in the Netherlands), or by ship (c.f. the planned Northern Lights project in Norway). If one would assume a 2 to 3 km deep offshore reservoir, reservoir – and thus wellbore – temperatures would be 80 to 120 °C (Eiken et al., 2011; Lescanne et al., 2011; Yoo et al., 2013), whereas the CO_2 would be injected with the water temperature, which can be as low as 0 °C. This implies that periodic injection could then lead to temperature fluctuations as much as 100 °C. Under such temperature fluctuations, the wellbore and subsurface formations may undergo cyclic shrinkage upon injection of cold CO_2 and subsequent expansion after injection when the system equilibrates back to reservoir temperature. As a result, as shown in Fig. 1, it is postulated that micro-annuli between wellbore casing, cement sheath, and

* Corresponding author at: Kai Li, Department of Geoscience & Engineering, Stevinweg 1, 2628 CN Delft, the Netherlands
E-mail address: K.Li-2@tudelft.nl (K. Li).

https://doi.org/10.1016/j.ijggc.2024.104103
Received 19 May 2023; Received in revised form 25 January 2024; Accepted 25 February 2024
Available online 8 March 2024

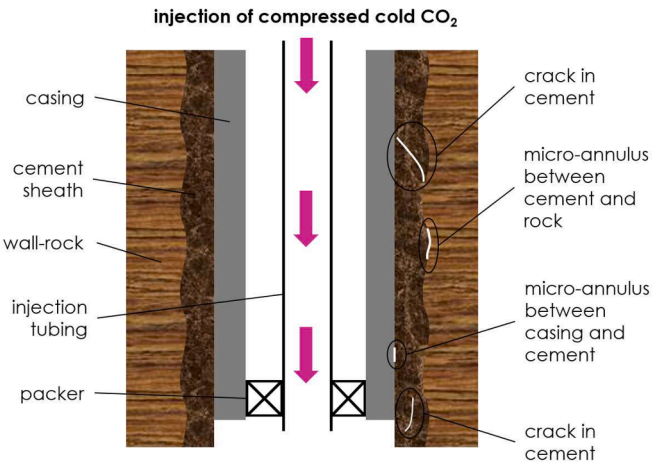

Fig. 1. Micro-annuli between wellbore casing, cement sheath, and wall-rock, and cracks in cement induced by injection of cold CO_2 and storage afterward.

wall-rock, and cracks in the cement may be induced (Carpenter et al., 1992; Carey et al., 2007; Roy et al., 2016; Vilarrasa and Rutqvist, 2017). The leakage of CO_2 through these pathways has been identified as one of the main challenges to securing safe and sustainable geological storage of CO_2 (Celia et al., 2005). Therefore it is of significance to understand how cement sheath integrity is affected by thermal cycling or shocks encountered in CCS.

In most depleted oil and gas wells targeted for CCS, ordinary Portland cement (OPC) is the main sealant composition, as it generally performs well as a zonal isolation material at relatively low costs in oil and gas industries (Parker et al., 2009; Santra and Sweatman, 2011; Lesti et al., 2013). However, the sealing integrity of wellbore using OPC-based sealant can be vulnerable and prone to deteriorate under strong temperature fluctuations during cyclic CO_2 injection and storage afterward. Albawi et al. (2014) conducted experiments with micro-computed tomography (micro-CT) to study the effects of thermal cycling on the integrity of a wellbore sample consisting of casing pipe, OPC-based sealant, and rock. Their sample was downscaled with a factor of 4 from a real wellbore section with a 311 mm borehole and 244 mm casing. They found thermal cycling at a temperature fluctuation amplitude of 75 °C caused leakage pathways up to several millimeters thick by debonding at casing/cement and cement/rock interfaces. Lund et al. (2015) performed simulations by considering the thermal properties of casing, cement, and rock to model the study by Albawi et al. (2014). They concluded that the integrity of the sample under thermal cycling was dependent on the thermal properties of all components of the sample. Large temperature fluctuations may lead to significant thermal stresses which could possibly damage the cement. De Andrade et al. (2015) also carried out experiments on a wellbore sample with the same configuration and dimensions as the one used by Albawi et al. (2014) to study the effects of thermal cycling. They concluded that shear failure was the most relevant mechanism for the debonding at interfaces. They further pointed out that, compared to sandstone, shale can better withstand thermal cycling, due to its higher stiffness and therefore greater resistance toward shear failures. All studies to date focused on sealing ability at the interfaces between casing, cement, and rock, while the integrity of the cement material itself when it undergoes thermal shocks remains unknown.

Besides OPC-based sealants, the efficacy of other alternatives under such temperature fluctuations is still unclear. Therefore, for future CCS wells, seeking improved wellbore sealing materials and testing their suitability to maintain enhanced long-term wellbore integrity is imperative. For example, calcium aluminate cement (CAC) becomes more and more popular, as it has a significantly higher early strength gain and a higher heat of hydration than OPC (Barborak, 2010). These characteristics make it attractive in the construction of future wells for CCS. Dugonjic-Bilic et al. (2011) tested the performance of a sealant composition based on CAC with a retarder in a CO_2 environment. They found that the ability of their composition to control water loss is suitable in CCS applications. However, how this sealant composition behaves under thermal cycling or shocks is still unknown.

In our study, we expose four sealant compositions, including existing and newly-designed OPC blends, and CAC blend, to high-frequency and abrupt cyclic thermal shocks of 100 °C by either quenching or flow-through experiments to study their integrity and suitability for CCS applications. To demonstrate the effects of thermal shocks on the sealants, we conduct mechanical tests and microstructural scanning on sealants before and after thermal treatment. Different sealants will have different thermal properties, which for most of the sealants tested in this study were thus far unknown. In addition, novel in the wellbore cement community, therefore thermal properties are measured for these four sealants, which ultimately aids in explaining the thermo-mechanical interaction observed in our experiments.

2. Experimental materials, apparatus, and methodologies

In our study, two sample types are used: solid cylindrical samples (Φ3 × 7 cm) and samples of the same dimensions but with a Φ4 mm central borehole along the vertical axis. The latter mimics a sealant with a pre-existing leakage pathway. Sealant samples are of four different compositions (see Table 1), namely S1: standard OPC-based blend, S2: ultra-low permeability OPC-based blend, S3: OPC-based blend with CO_2-sequestering additives, and S4: CAC-based blend. These sealants include representatives of currently-used wellbore sealing materials in old oil and gas wells considered for CO_2 storage (S1 and S2, as references), and designed blends, targeted for newly drilled CCS wells (S3 and S4). Table 1 shows an overview of the four different sealant compositions and their respective technology readiness levels (TRL's).

For cementitious materials, it can take years to complete their strength-gaining process (Neville and Brooks, 1987). All samples used in this study are prepared by Halliburton AS Norway, in accordance with API Recommended Practice 10B-2 (API RP 10B-2, 2013). This includes a water/cement ratio of 0.4, and curing at 150 °C and 30 MPa for 28 days. The high temperature and pressure ensure that most chemical reactions have gone to near completion after curing, and as such it ensures that the mechanical and thermal properties of our samples will not vary significantly during the study duration. After curing, all samples are submerged in fresh water and stored at room temperature until use. In our study, all samples are completely dried before each experiment in an air-circulated oven (model UF75, Memmert). Samples are placed in the room temperature oven, and we first apply a ramping rate of 2.5 °C/min to heat the sample to 80 °C and leave the sample at 80 °C for 2 days. After complete dewatering, we then cool the sample down to room temperature at the same ramping rate. These procedures ensure that associated thermal stresses during heating and cooling are least abrupt, and cause no damage to the sealing ability of the sample. After cooling down, we then measure the bulk density of the dried sealants of all four

Table 1
an overview of four sealant compositions and their TRL's.

Sealant	Composition	TRL
S1	1.90 SG class G cement with 35 % BWOC silica flour	7: proven technology
S2	1.90 SG ultra-low permeability class G cement with 35 % BWOC silica flour, with silica fume and expansion agent in form of dead-burnt MgO	7: proven technology
S3	1.90 SG class G cement with 35 % BWOC silica flour, with silica fume, expansion agent in form of dead-burnt MgO, and CO_2-sequestering additives	3: prototype tested
S4	1.80 SG calcium aluminate cement-based blend	7: proven technology

compositions.

Before any thermal-shocking experiments, we determine the mechanical and thermal properties of the four sealants (Table 2). We perform unconfined compression tests to measure unconfined compression strength (UCS), Young's modulus, and Poisson's ratio of intact samples, both solid ones and those with a borehole. Mechanical testing is carried out using a 500 kN loading frame. Displacement is controlled with two high-precision linear variable differential transformers (LVDTs) with a 2 mm range, and on the sample a circumferential strain gage is mounted with a 10 mm range. All UCS tests are carried out in displacement control mode with a ramping rate of 0.0005 mm/s, corresponding to a strain rate of 7.1×10^{-6}/s. Furthermore, we use a thermal constants analyzer (Hot Disk® TPS 2200) to measure the thermal conductivity and specific heat capacity of the dried sealant samples. The thermal diffusivity, a, which describes the ability of the sealant to conduct thermal energy relative to its ability to store thermal energy, can then be calculated by:

$$a = \frac{\lambda}{\rho c} \quad (1)$$

where λ is the thermal conductivity of the sealant, ρ the bulk density of the dried sealant sample, and c the specific heat capacity.

Note that all properties of solid samples of each sealant composition listed in Table 2 are averaged based on measurements of three samples each made at an interval of one month. The relatively small standard deviation implies that our measurements are repeatable, and the mechanical and thermal properties of sealants have not changed throughout our study duration. The mechanical properties of samples with a borehole are almost the same as solid samples. This is probably because the borehole is too small compared to the sample, with a sectional area ratio of 1.8 %, to substantially impact sealant mechanics. Table 2 also gives the water permeability of the four sealants, as measured at 80 °C by Halliburton AS Norway, where each permeability test takes 3 to 6 months.

To quantify the effects of thermal shocks on the sealants, we use an X-ray micro-tomography (micro-CT) scanner (model Nanotom 180 NF, Phoenix X-ray Systems & Services GmbH) to scan samples at a voxel resolution of 32 μm. We then use Phoenix datos software (version 2.0, GE Measurement & Control solutions) to post-process the images and further use Avizo software (version 2020.2, ThermoFisher Scientific) to construct the 3D microstructure of cracks and voids in samples before and after experiments. Due to the limitation of our technique, microcracks and voids of size below 32 μm cannot be detected. The workflow of image analysis is detailed in the Appendix. In addition, we measure the UCS of samples after the experiments to study how these thermal-induced cracks and voids affect sealant integrity. Table 3 shows all samples to be tested and their respective experimental schemes.

In our experiments, we adopt two experimental approaches to study the effects of thermal shocks on sealant integrity. We either quench preheated solid sealant samples (type 1) or flow cold water through the preheated samples with a central borehole (type 2). Fig. 2 shows the procedure for the two approaches.

In type 1 quenching experiments, we first heat the sample to 120 °C and maintain it at this temperature for half an hour in the oven, and then quickly transfer the sample into a 6 L 20 °C cold water bath. After that, the sample is reheated to 120 °C within 12 mins in the oven for the next shock. This is repeated eight times. However, it should be noted that such abrupt and high-frequency temperature fluctuations are unlikely in field operations. We adopted these harsh experimental conditions to

Table 3
an overview of all samples to be tested and their respective experimental schemes. Quenching is type 1 testing, and flow-through is type 2 testing.

No.	Sample name	Sealant composition	Sample configuration	Experimental schemes
1	S1–1	S1, OPC blend	Solid	micro-CT → quenching → micro-CT → UCS
2	S1–2			
3	S1–3		With a borehole	micro-CT → flow-through → micro-CT → UCS
4	S2–1	S2, OPC blend with ultra-low permeability	Solid	micro-CT → quenching → micro-CT → UCS
5	S2–2			
6	S2–3		With a borehole	micro-CT → flow-through → micro-CT → UCS
7	S3–1	S3, OPC blend with CO_2-sequestering additives	Solid	micro-CT → quenching → micro-CT → UCS
8	S3–2			
9	S3–3		With a borehole	micro-CT → flow-through → micro-CT → UCS
10	S4–1	S4, CAC blend	Solid	micro-CT → quenching → micro-CT → UCS
11	S4–2			
12	S4–3		With a borehole	micro-CT → flow-through → micro-CT → UCS

Table 2
mechanical and thermal properties as measured before thermal shocking, and permeability of the four sealants (provided by Halliburton AS Norway).

Sealant	Unconfined compressive strength [MPa]	Young's modulus [GPa]	Poisson's ratio [-]	Bulk density [kg/m^3]	Thermal conductivity [W/(m·K)]	Specific heat capacity [J/(kg·K)]	Thermal diffusivity [mm^2/s]	Water permeability [μDarcy]
S1, solid	98.6 ± 1.1	13.5 ± 0.3	0.157 ±0.002	1455	0.82±0.04	878±18	0.64	0.14
S1, with borehole	99.8	13.44	0.143					
S2, solid	80.3 ± 1.4	12.6 ± 0.1	0.153 ±0.010	1507	0.93±0.03	936±11	0.66	0.00005
S2, with borehole	81.1	12.0	0.162					
S3, solid	33.3 ± 0.9	6.1 ± 0.1	0.124 ±0.007	1374	1.04±0.02	684±13	1.11	0.014
S3, with borehole	33.4	6.1	0.139					
S4, solid	35.3 ± 1.4	6.5 ± 0.1	0.157 ±0.013	1497	0.89±0.02	970±21	0.61	0.32
S4, with borehole	34.3	6.6	0.172					

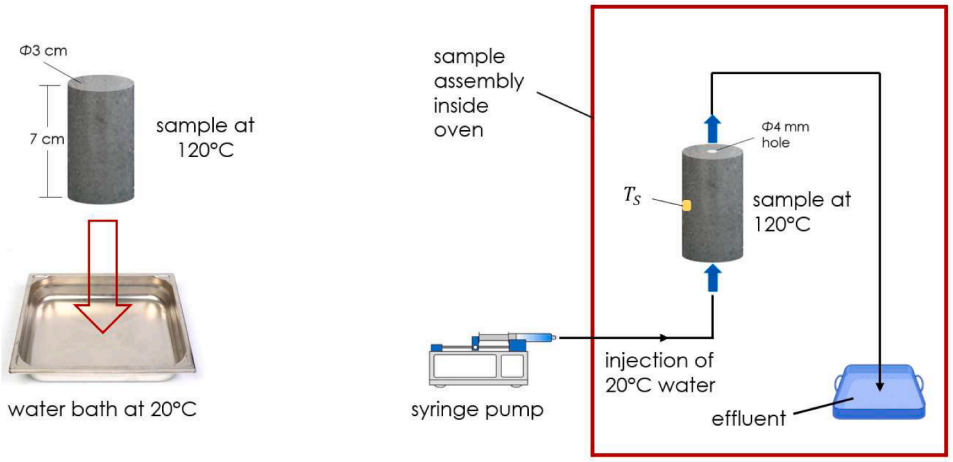

Fig. 2. left. Procedure for type 1 quenching experiments; **right**. Procedure for type 2 flow-through experiments.

amplify the impacts of thermal shocks on our sealants whilst maintaining a feasible procedure on a laboratory time-scale. For each sealant composition, we performed quenching experiments on two individual samples, by which the second sample for each sealant was tested at least three months after the first one.

In type 2 flow-through experiments, we mount two stopcocks with luer connectors (EW-300600–00, VWR, the Netherlands) on the sample (with a central borehole) to build the inlet and outlet, which are then linked with the flowline to allow the injection. During the experiment, the whole sample assembly (unjacketed and unconfined) is placed in the oven at 120 °C. After the assembly stays at this temperature for half an hour, we use a syringe pump (model 1000D, Teledyne ISCO) to inject 160 mL 20 °C water through the sample from bottom to top in 2 min to apply a strong thermal shock. We then halt for 12 min before the next injection to allow the sample to heat up again. As shown in Fig. 2 (right), a thermocouple (type K, NI-9219, National Instruments, max. reading 700 °C, accuracy ±1 °C) is mounted in the middle on the outer surface of the sample to measure the temperature, T_s, during the experiment. In type 2 experiments, we also performed eight cycles of thermal shock, and we tested one sample for each sealant composition.

In addition, we carry out reference experiments to investigate the effects of water exposure, by applying eight wet/dry cycles on one solid sample of each sealant composition. This allows us to examine how the process of repeated drying and wetting during both types of thermal-shocking experiments alone affects the sealant integrity. In each wet/dry cycling experiment, we first dry the sample at room temperature for 10 h, then soak it in room temperature water bath for 2 min before the next drying, i.e. the equivalent of the quenching procedure, without the thermal effects. After the wet/dry cycling, we measure the UCS's of the four samples of different compositions.

3. Results

3.1. Effects of thermal shocks on the microstructure of sealant samples

Figs. 3–6 show the microstructure of the two samples before and after type 1 quenching experiments for each of the four sealant compositions S1 to S4, respectively. These images show the structure of cracks and voids (of size larger than 32 μm) in samples, where interconnected cracks are displayed in the same color. Samples of S1 and S3 compositions have voids before quenching (Figs. 3 and 5). Samples of S2 and S4 do not have pre-existing voids of size larger than 32 μm, so orthogonal slices are given in Figs. 4 and 6 to illustrate the intactness of the samples before quenching.

For sealants S1, S2, and S4 (Figs. 3, 4, and 6), type 1 experiments induced cracks and voids in both samples. In sealant S1 the quenching procedure led to some connected cracks and a significant increase in void volume, and in S2 some connected cracks and some new voids were created. Sample S4 shows sample-size connected cracks, and only a few disconnected new voids after quenching. This means quenching generated abrupt and sufficient thermal stresses to cause cracking in the cement of these three compositions. By quenching, multiple cracks and new voids developed at different orientations and locations throughout the sample, where in sample S4–2 (Fig. 6) all thermally-induced cracks are connected to form a potential leakage pathway for flow. Note that both S4 samples are still cohesive after quenching, despite the sample-size connected cracks. On the contrary, both samples of S3 are intact after quenching, and show no obvious changes.

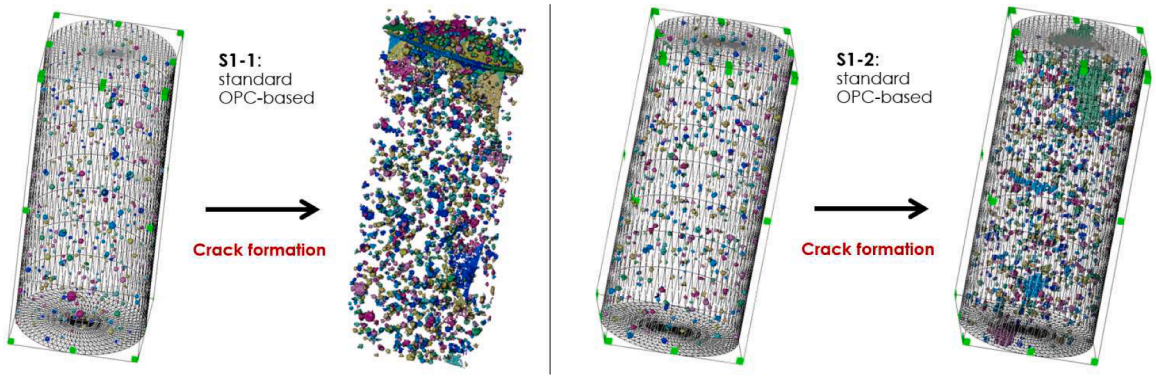

Fig. 3. Microstructure of samples S1–1(left) and S1–2 (right) before and after quenching. Voxel resolution of 32 μm. Samples are of sealant composition S1, standard OPC-based. Some connected cracks and many new voids develop in both samples.

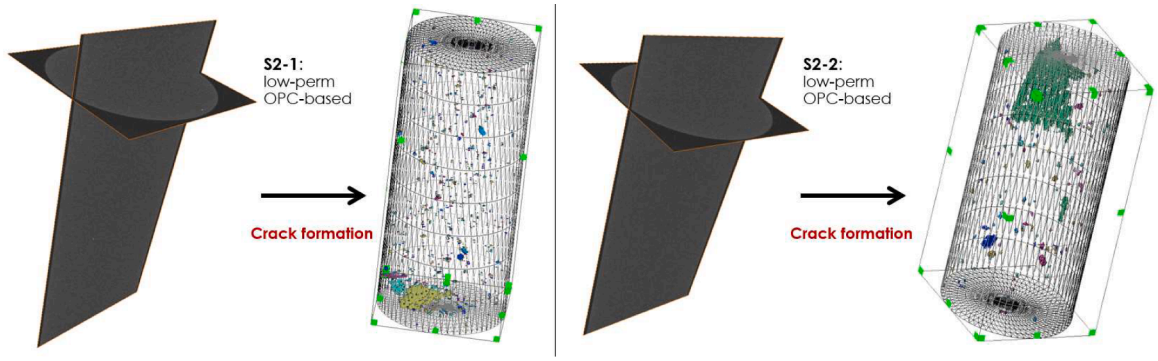

Fig. 4. Microstructure of samples S2–1(left) and S2–2 (right) before and after quenching. Voxel resolution of 32 μm. Samples are of sealant composition S2, low-permeability OPC-based. Some connected cracks and visible new voids develop in both samples.

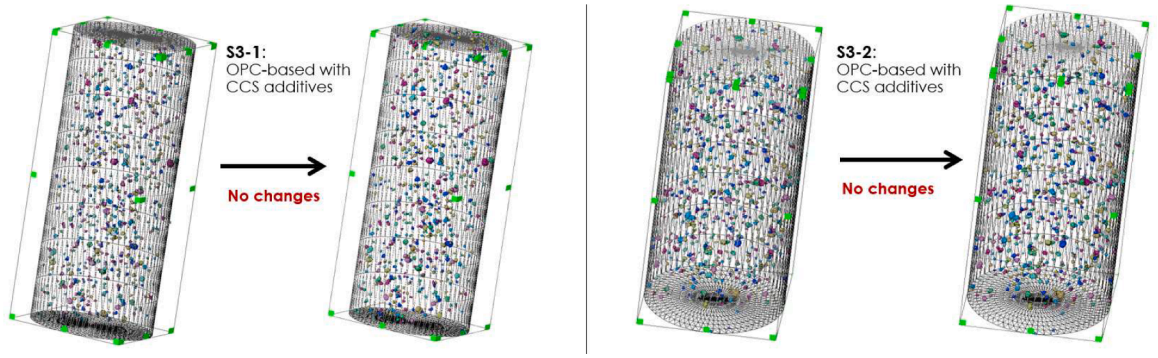

Fig. 5. Microstructure of samples S3–1(left) and S3–2 (right) before and after quenching. Voxel resolution of 32 μm. Samples are of sealant composition S3, OPC-based with CCS additives. There are no obvious changes after quenching in either sample.

Fig. 6. Microstructure of samples S4–1(left) and S4–2 (right) before and after quenching. Voxel resolution of 32 μm. Samples are of sealant composition S4, CAC-based. Connected cracks and occasional new voids develop in both samples.

Fig. 7 shows the structure of voids and cracks in samples of all four sealant compositions before and after type 2 flow-through experiments. Type 2 experiments also induced cracks and new voids in samples of sealants S1, S2, and S4. However, compared to quenching, only limited cracks (all radial) were created in these sealants by flow-through. These radial cracks all intersect with the borehole of the sample. In sample S1–3, the flow-through procedure created two major radial cracks and significant new voids. In sample S2–3, only one radial crack close to the injection inlet and some voids were created. And in sample S4–3, a sample-size radial crack and few voids developed after the experiment. Like in quenching for sample S4–2, flow-through created cracks also all through sample S4–3. Despite the cracks in S1, S2, and S4, we haven't observed any water flowing out of the sample surface during the experiment. In low-porosity geological formations, fractures form high-permeability pathways (Bense et al., 2013). Therefore, in our study, the presence of thermally-induced cracks in S1, S2, and S4 indicates that these sealants have lost their sealing ability. In contrast, the flow-through procedure caused no obvious changes for sample S3–3.

To study quantitively to what extent thermal-shocking experiments (both type 1 and type 2) affect sealant samples, we use Avizo software to calculate the volume of the cracks and voids in the samples (see Appendix for detailed workflow). Fig. 8 compares this volume for each sample of the four sealant compositions before and after the experiment.

As shown in Fig. 8, the volume of cracks and voids for intact samples of sealants S2 and S4 are zero, as those samples are compact with no pre-existing voids of size larger than 32 μm. The volume of cracks and voids increases for all samples of sealants S1, S2, and S4 after experiments, while it stays the same for S3 samples. In general, the observed volume increase for S1, S2, and S4 is bigger for type 1 quenching than for the type 2 flow-through experiments. By quenching the relatively small

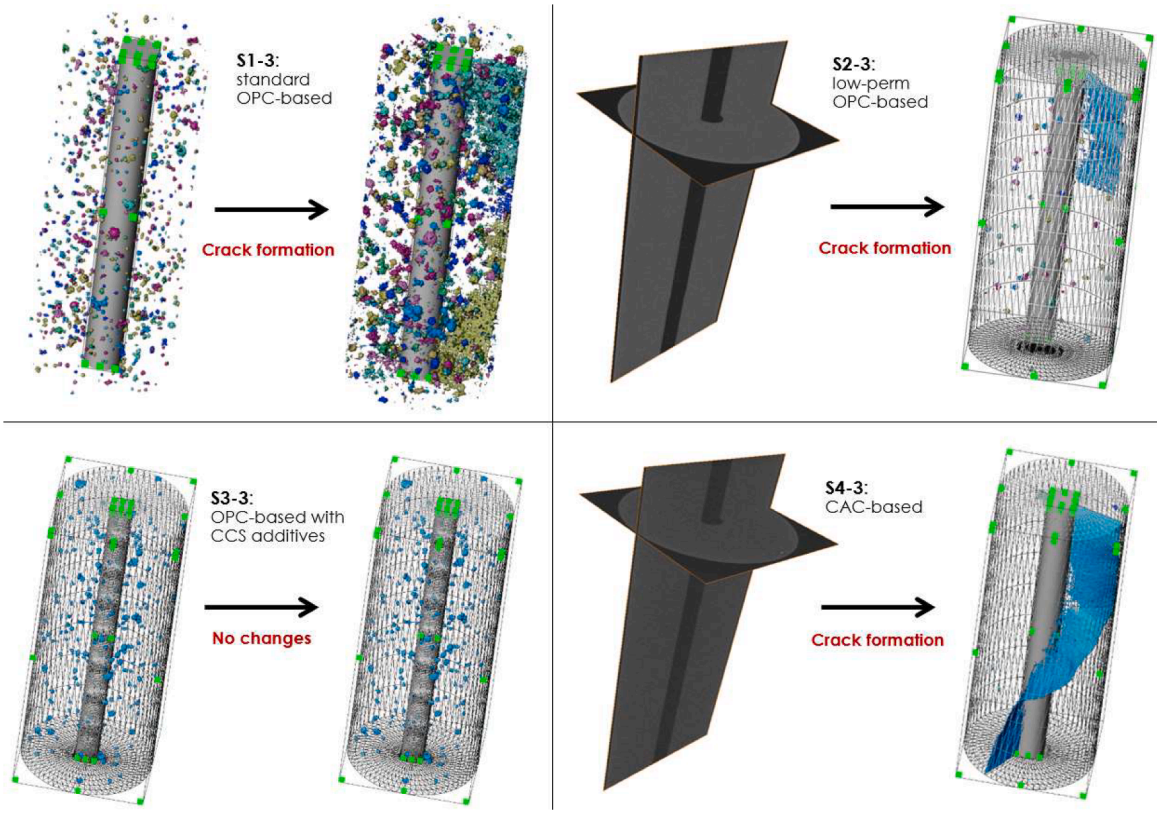

Fig. 7. Microstructure of samples S1–3 (sealant S1, upper left), S2–3 (sealant S2, upper right), S3–3 (sealant S3, bottom left), and S4–3 (sealant S4, bottom right) before and after flow-through experiments. Voxel resolution of 32 μm. The injection inlet is at top, and outlet at bottom of these four sample illustrations. Radial cracks and new voids develop in sealant types S1, S2 and S4, whereas in sample S4–3 the crack is sample size. Sealant S3 shows no obvious changes after the flow-through experiment.

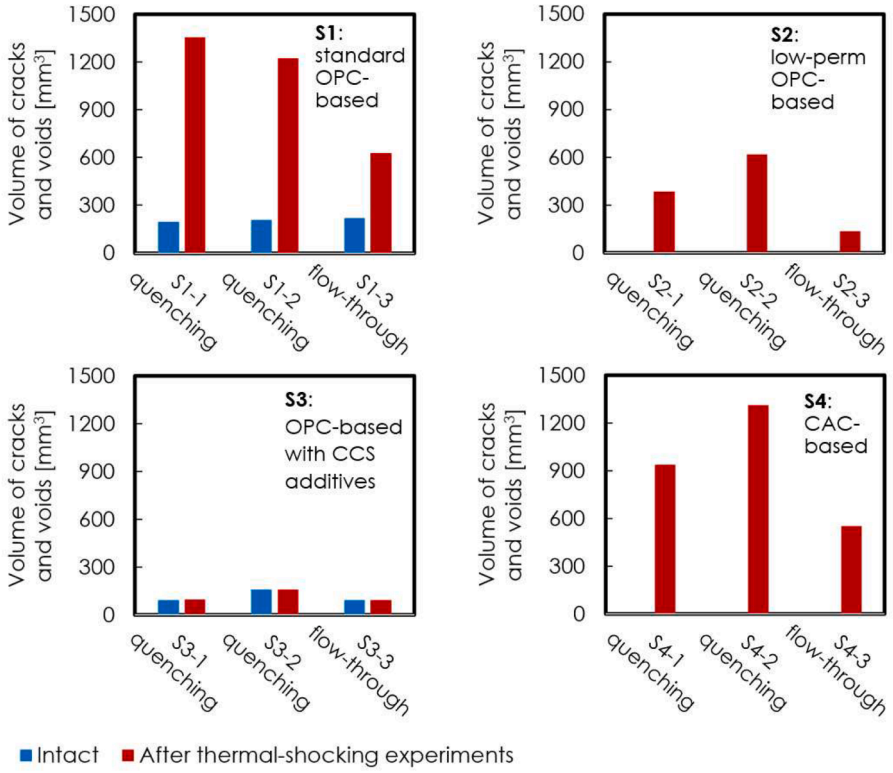

Fig. 8. Volume of cracks and voids for each sample of the four sealant compositions before and after thermal-shocking experiments. The volume for intact samples of sealants S2 and S4 are zero, as those samples are compact with no pre-existing voids of size larger than 32 μm.

sample in a 6 L cold water bath, the entire outer surface of the sample experiences an extreme and instantaneous temperature difference, creating a relatively large thermal shock effect. The maximum temperature gradient from outside to inside of the sample is therefore attained, which then creates large thermal stresses abruptly to break the sample. In contrast, in flow-through experiments, we flush 160 mL cold water through the small central borehole of the sample in 2 mins during each cycle of thermal shock. The smaller surface area in contact with cold water means that the potential for thermal stresses is much lower than by quenching. Moreover, any stresses which occur are in the radial direction and located in the vicinity of the borehole. The temperature of the water also increases as it flows through the borehole. In type 2 flow-through experiments, hence, the temperature fluctuation near the inlet of the borehole is greater than that near the outlet, which implies that more abrupt and larger thermal stresses are created nearby the inlet. All aforementioned mechanisms explain why for S1, S2, and S4 there are more thermally-induced cracks and voids by quenching than by flow-through. Moreover, by quenching, they are at different orientations throughout the sample, while by flow-through fewer and only radial cracks develop and intersect with the borehole in samples.

3.2. Effects of thermal shocks on ucs of sealant samples

In addition, after micro-CT scanning, we measure the unconfined compressive strength (UCS) for each sample. The changes in the UCS are direct consequences of the thermal treatment. Fig. 9 shows how UCS changes after thermal shocks for the four different compositions and for the two different procedures.

As shown in Fig. 9, the UCS of sealants S1, S2, and S4 decreases after both types of thermal-shocking experiments, where the decrease for the quenching treatment is larger than the decrease for the flow-through treatment. The variability in UCS's for the repeat experiments is 5–11 MPa (shown in red diamonds in Fig. 9), which is much less than the difference between the intact strength and the strength after either thermal-shocking procedure. For sealants S1, S2, and S4, the reduction in UCS after quenching (by 41 %, 50 %, and 67 % on average for S1, S2, and S4 samples, respectively) is greater than after flow-through (by 19 %, 27 %, and 40 % for samples S1–3, S2–3, and S4–3, respectively). This relates to the changes in the volume of cracks and voids due to thermal shocks (Fig. 8): for each sealant, the larger increase in the volume of thermal-induced cracks and voids leads to a greater reduction in strength. Furthermore, for sealant S3, there is no substantial change in the UCS after thermal shocks by flow-through (see S3–3 in Fig. 9). Counter-intuitively, samples S3–1 and S3–2 become on average 47 % stronger after quenching. Also note that even with a greater reduction in UCS after quenching, S1 and S2 still exhibit higher UCS than intact S3 and S4 sealants.

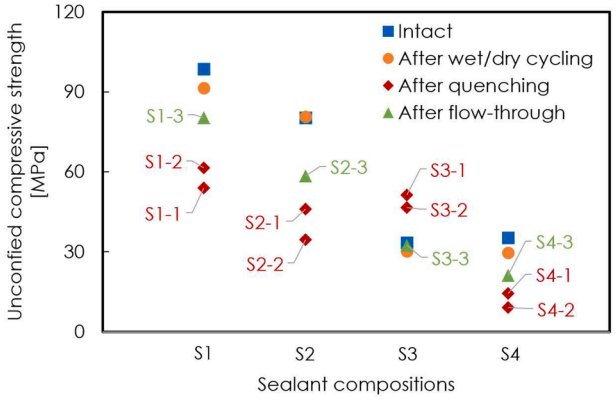

Fig. 9. UCS of samples of the four sealant compositions before and after thermal-shocking experiments.

Fig. 9 also displays the UCS's of samples of the four different compositions after eight room temperature wet/dry cycles. The UCS shows a slight decrease for sealants S1, S3 and S4 (by 7 %, 9 % and 16 %, respectively), whereas it shows insignificant change for sealant S2. Note that this strength loss in sealant S1 and S4 is insignificant compared to the strength loss by either quenching or flow-through experiment. After wet/dry cycling, all samples were visually intact, so no observable cracks were created.

3.3. Temperature profile in type 2 experiments

During type 2 flow-through experiments, we measured the temperature, T_s, in the middle on the outer surface of the sample (Fig. 2). We then use this temperature to calculate the amplitude of temperature fluctuation due to thermal shocks since the outset of the first shock (after the sample is maintained at 120 °C for half an hour), by $(T_s - 120)$ °C. Fig. 10 shows the amplitude of temperature fluctuation during the eight cycles of thermal shocks in flow-through experiments for the four samples of different compositions.

Upon each cycle of thermal shock, the temperature at the outer surface of all four samples first drops until it reaches the maximum temperature fluctuation amplitude at the end of the injection of cold water. The temperature then gradually rises back to equilibrate with the system temperature before the next shock. As the cycles progress, the samples gradually cool down where S1–3 and S4–3 usually get closest to their original temperature, followed by S3–3. S2–3 stays furthest away from the original temperature, about 0.5 °C. Throughout all eight cycles of thermal shocks, the average maximum amplitude of temperature fluctuation is 5.1, 6.1, 7.4, and 4.5 °C for samples S1–3, S2–3, S3–3, and S4–3, respectively.

Essentially, these temperature drops during cold-water injection phases for all four samples in type 2 experiments signify that heat has transferred from the outer part of the sample toward the central borehole. All four samples experience the same boundary conditions with respect to sample temperature prior to flow-through, the amount, temperature and the rate of injected water. Therefore, this flux of thermal energy during thermal shocks can only be governed by the thermal properties of the sealants, specifically the thermal diffusivity. Heat should transfer more rapidly in a material with a higher thermal diffusivity. Fig. 11 displays the relationships between the maximum amplitude of temperature fluctuation, thermal diffusivity of samples, and the fraction of UCS reduction in type 2 flow-through experiments for the four samples. Sample S3–3 shows the highest temperature fluctuation,

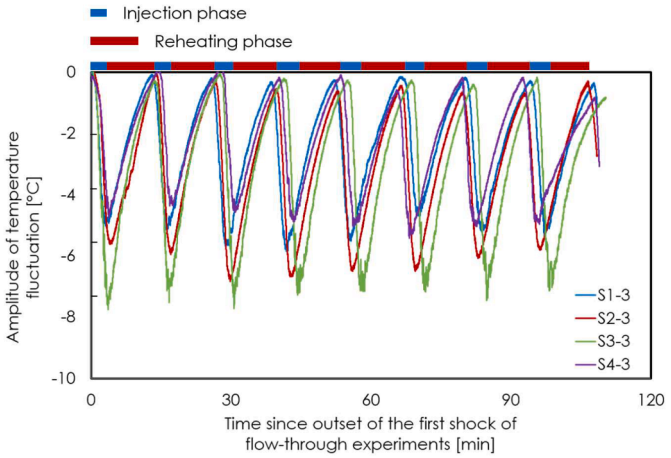

Fig. 10. Amplitude of temperature fluctuation during eight cycles of thermal shocks in type 2 flow-through experiments for samples of the four compositions. Time zero marks the outset of the first shock. Samples are maintained at 120 °C for half an hour before time zero.

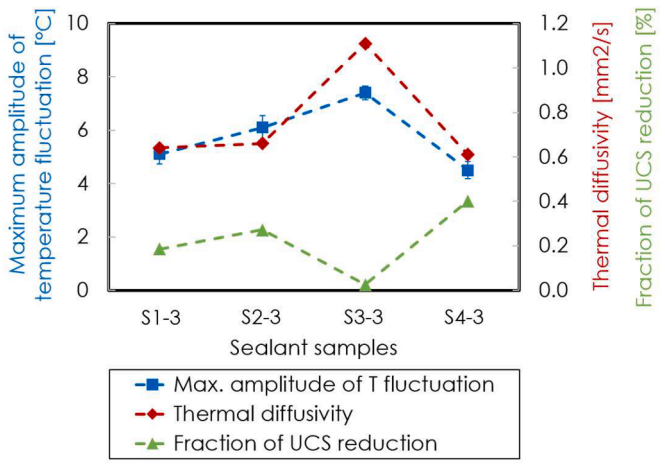

Fig. 11. Relationships between the maximum amplitude of temperature fluctuation, thermal diffusivity of samples, and the fraction of UCS reduction in type 2 flow-through experiments for the four samples of different compositions.

and the least strength reduction. It also has the highest thermal diffusivity. We postulate that due to the high thermal diffusivity less thermal stresses built up, and that therefore less damage results from high temperature fluctuations during thermal cycles. This would explain why sample S3–3 was undamaged after thermal shocks.

4. Discussion

In this study, we tested sealant samples of four compositions to study their sealing ability under thermal shocks for CCS applications. In our study, in addition to two reference OPC-based sealants (S1 and S2), we also tested two blends with different compositions designed for future CCS wells (S3 and S4). S3 is based on OPC but with CO_2-sequestering additives, and its integrity was not compromised after the flow-through experiment, and even enhanced after quenching. The additives in S3 encapsulate crushed peridotite material primarily composed of olivine (Kvassnes and Clausen, 2020, 2021). In a CO_2-rich environment, magnesium silicates in olivine can be carbonized to magnesium carbonate, which enhances the self-healing ability of the cement. All these position S3 as an optimal candidate for a sealant in CCS wells. In a CO_2-rich environment, it is anticipated that a mere 2 % by weight of olivine in cement can yield substantial initial reactions upon CO_2 exposure, providing early buffer capacity, restricted volume compensation, and initial resistance to CO_2. However, in our experiments we have not added additional CO_2, neither during the curing process nor during the mechano-thermal experiments. Exactly what mineralogical changes have taken place in sealant S3 which gives it its favorable thermal properties during these experiments are unknown. The current work demonstrates that the thermal properties are essential for the capacity of a sealant to deal with thermal shocks and hence for suitability in a CCS context. Sealant S4 is based on calcium aluminate cement (CAC), and all S4 samples fully lost integrity after both types of thermal shocks. Compared to OPC, CAC contains a far greater amount of alumina (>90 %) and a far less amount of silica (Barborak, 2010). Even though CAC gains significantly higher early strength during its curing process, it may undergo a conversion process later where a strength loss of 50 % or more is possible (Adams and Ideker, 2017; Son et al., 2018). This process happens when metastable phases of the hydration products convert to more stable ones.

There are three important limitations to this work. First, we implemented eight abrupt sequential temperature drops, especially by quenching, on samples that is unlikely to be encountered in field cases. In other experimental studies (Albawi et al., 2014; De Andrade et al., 2015; Lund et al., 2015), temperature dropped by 70 to 90 °C with a smaller ramping rate (1.5 to 2.3 °C/min) than ours were applied to achieve cyclic temperature fluctuation on cement samples. All these severe conditions are not representative in the field, where temperature in the subsurface would vary less and at a more gradual rate than ours. We applied these harsh experimental conditions to augment the damaging impacts of thermal shocks on our sealants, then to be able to evaluate their durability under thermal loads by measurable difference on a laboratory time-scale.

Second, our samples started out dry, and became progressively more water-saturated with each thermal shock. However, our wet/dry cycling reference experiments showed that the integrity compromise for sealants S1, S2 and S4 by both types of thermal-shocking experiments is substantial compared to any mechanochemical changes due to water exposure alone. Torsæter et al. (2017) studied the integrity at the interface between cement and rock by applying thermal shocks to the sample with liquid nitrogen. They found that a dried sample remained intact and a wet sample lost its integrity after thermal shocks. Yet it is still not clear how wet samples of our sealant compositions behave under thermal shocks. This topic deserves further study.

Last, all experiments were conducted at a worst-case scenario with zero confinement, whereas at CO_2 storage depths (e.g. 1 km, Kirby et al., 2001; Alnes et al., 2011; Zhang et al., 2022) we expect cement to experience a confining pressure up to 10 MPa based on lithostatic pressure. In such a case, the presence of confinement should avoid or at least mitigate the adverse effects of thermal stresses on sealing ability of the cement. The confinement is expected to provide support to the sealant sample and increase its stiffness, hence reducing the potential for thermally-induced cracks in the cement. This is in line with what De Andrade et al. (2015) have found. In their experiments, they applied 10 thermal cycles from 130 to −5 °C on a wellbore section analogue that included casing, cement and rock. They concluded, compared to unconfined experiments, the presence of confining pressure reduced the occurrence of cracks within the cement sheath due to thermal cycling loads. Brittle fracturing is in general a dilative process, and it therefore stands to reason, demonstrated by the findings of De Andrade et al. (2015), that the presence of confining pressure, which would be expected along most if not all of the wellbores, would suppress the formation of open fractures. Thus, this work, even though it clearly highlights the importance of the interplay between thermal properties, strength and expected resilience in CCS settings, is limited by omitting the effects of confining pressure. Future work is needed to address this.

5. Conclusions

In this study, we conducted two types of experiments to investigate the type and extent of thermal damage and what its effects are on the integrity of sealants of four different compositions. These sealants include reference OPC (ordinary Portland cement)-based blends (S1, based on standard OPC, and S2, based on OPC with ultra-low permeability), newly-designed blend (S3, based on OPC with CO_2-sequestering additives), and CAC (calcium aluminate cement)-based blend (S4).

We found that samples of sealants S1, S2, and S4 lost sealing ability due to fractures after both types of thermal-shocking experiments, indicating that these compositions may not be optimal candidates for well-sealing materials for CCS. For all these three sealants, quenching displayed more jeopardizing effects than flow-through experiments. By quenching, cracks and new voids developed throughout the samples at different orientations and caused a decrease in UCS by 41 % (41 MPa), 50 % (40 MPa), and 67 % (24 MPa) on average for samples of S1, S2, and S4 compositions, respectively. In flow-through experiments, only a limited number of radial cracks that intersected with the borehole, and voids were initiated. UCS decreases by 19 % (18 MPa), 27 % (22 MPa), and 40 % (14 MPa) for S1, S2, and S4 samples, respectively. This is because, by quenching, a larger surface of the sealants was exposed to a high temperature difference, i.e. creating a more severe thermal shock. In such a case, thermal stresses were accumulated more abruptly which

resulted in larger adverse effects on sealant integrity. It is also of practical significance to note that, even with a greater reduction in UCS after quenching, S1 and S2 still exhibit higher UCS than intact S3 and S4 sealants (Fig. 9).

However, we have not observed any thermally-induced cracks in samples of sealant S3 after experiments. The flow-through experiment caused no significant changes in the S3 sample, and quenching even somewhat enhanced the integrity of this sealant with an increase in strength. We postulate that this is mainly caused by the higher thermal diffusivity of sealant S3 compared to the other three sealants. The increased efficiency of heat transfer throughout the sample led to thermal stresses less abruptly, insufficient to damage the integrity of S3 samples. This work clearly demonstrates the importance of knowing the thermal properties of the sealants used in the wellbores in designing subsurface CO_2 storage sites.

Our study furthermore implies that standard OPC-based sealants used in most of the currently existing wells and the CAC-based sealant designed for future CCS wells may be susceptible to potential challenges when subjected to extreme thermal shocks that are comparable to ours during cyclic CO_2 injection and storage afterward. Upgrading sealant materials to prevent or mitigate the adverse effects of thermal shocks and maintain long-term wellbore sealing integrity during CCS can be beneficial.

In short, this study provides a novel method to study existing and newly-designed sealants, and assess their integrity under strong thermal shocks in a worst-case scenario i.e. dry samples without confinement. We also applied a large temperature change at an abrupt rate on sealants, which is severe compared to likely conditions imposed on the cement sheath of CCS wells. Based on our results, we observed different thermally-induced cracking behaviors for sealants of different compositions, where we postulate that their thermal diffusivity is the key characteristic that determines the capacity of sealants to maintain sealing ability under thermal shocks.

CRediT authorship contribution statement

Kai Li: Writing – original draft, Validation, Methodology, Investigation, Formal analysis, Data curation. **Anne M.H. Pluymakers:** Conceptualization, Writing – review & editing, Supervision, Funding acquisition.

Declaration of competing interest

The authors declare that they have no known competing financial interests or personal relationships that could have appeared to influence the work reported in this paper.

Data availability

Data will be made available on request.

Acknowledgements

This study is a part of the CEMENTEGRITY project (project number: 327311) funded through the ACT program (Accelerating CCS Technologies, Horizon2020 project number 691712). The CEMENTEGRITY project aims to develop and test novel sealants that can better maintain wellbore integrity during CO_2 injection and storage afterward. Financial contributions from the Research Council of Norway (RCN), the Netherlands Enterprise Agency (RVO), the Department for Business, Energy & Industrial Strategy (BEIS, UK), and Wintershall DEA are gratefully acknowledged. We thank our consortium partners (IFE (Institutt for Energiteknikk), Halliburton AS Norway, ReStone AS, Universitet i Stavanger, EBN B.V., Heriot-Watt University, and Wintershall DEA) for their kind support to our study.

We thank Marc Friebel and Jens van den Berg in Rock Mechanics Laboratory at Delft University of Technology, the Netherlands, for their technical support.

Appendix

In this study, we use Phoenix datos software to post-process the images of each sample acquired by micro-CT scanning. We then use Avizo software to construct the 3D microstructure of cracks and voids in the sample. The workflow is shown below.

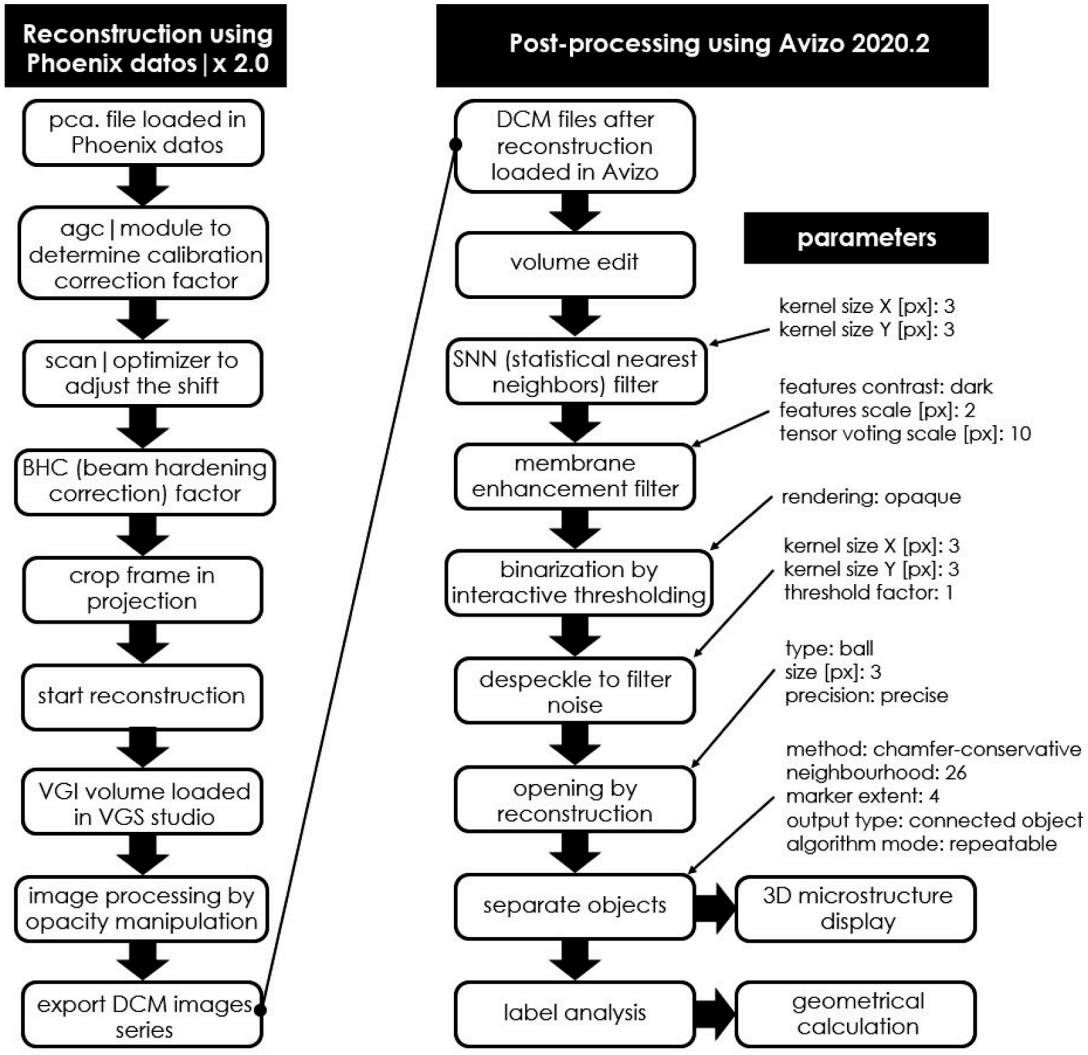

Workflow of image analysis.

References

Adams, M.P., Ideker, J.H., 2017. Influence of aggregate type on conversion and strength in calcium aluminate cement concrete. Cem. Concr. Res. 100, 284–296. https://doi.org/10.1016/j.cemconres.2017.07.007.

Albawi, A., De Andrade, J., Torsæter, M., Opedal, N., Stroisz, A., Vrålstad, T., 2014. Experimental set-up for testing cement sheath integrity in arctic wells. In: OTC Arctic Technology Conference. OnePetro. https://doi.org/10.4043/24587-MS.

Alnes, H., Eiken, O., Nooner, S., Sasagawa, G., Stenvold, T., Zumberge, M., 2011. Results from Sleipner gravity monitoring: Updated density and temperature distribution of the CO_2 plume. Energy Procedia 4, 5504–5511. https://doi.org/10.1016/j.egypro.2011.02.536.

API, R.P., 2013. 1.0b-2: Api Recommended Practice 10B-2, Recommended Practice For Testing Well Cements. API RP 10B-2.

Barborak, R., 2010. Calcium Aluminate Cement Concrete (class cac concrete) Txdot Special Specification ss-4491 Tip Sheet. Construction and Bridge Divisions, Texas Department of Transportation, Austin, TX, USA.

Bense, V.F., Gleeson, T., Loveless, S.E., Bour, O., Scibek, J., 2013. Fault zone hydrogeology. Earth Sci. Rev. 127, 171–192. https://doi.org/10.1016/j.earscirev.2013.09.008.

Budinis, S., Krevor, S., Mac Dowell, N., Brandon, N., Hawkes, A., 2018. An assessment of CCS costs, barriers and potential. Energy strategy reviews 22, 61–81. https://doi.org/10.1016/j.esr.2018.08.003.

Bui, M., Adjiman, C.S., Bardow, A., Anthony, E.J., Boston, A., Brown, S., Mac Dowell, N., 2018. Carbon capture and storage (CCS): The way forward. Energy Environ. Sci. 11 (5), 1062–1176. https://doi.org/10.1039/C7EE02342A.

Carey, J.W., Wigand, M., Chipera, S.J., WoldeGabriel, G., Pawar, R., Lichtner, P.C., Wehner, S.C., Raines, M.A., Guthrie Jr, G.D., 2007. Analysis and performance of oil well cement with 30 years of CO_2 exposure from the SACROC Unit, West Texas, USA. Int. J. Greenhouse Gas Control 1 (1), 75–85. https://doi.org/10.1016/S1750-5836(06)00004-1.

Carpenter, R.B., Brady, J.L., Blount, C.G., 1992. The effects of temperature and cement admixes on bond strength. J. Petroleum Technol. 44 (08), 936–941. https://doi.org/10.2118/22063-PA.

Celia, M.A., Bachu, S., Nordbotten, J.M., Gasda, S.E., Dahle, H.K., 2005. Quantitative estimation of CO_2 leakage from geological storage: Analytical models, numerical models, and data needs. In: Greenhouse Gas Control Technologies, 7. Elsevier Science Ltd, pp. 663–671. https://doi.org/10.1016/B978-008044704-9/50067-7.

De Andrade, J., Sangesland, S., Todorovic, J., Vrålstad, T., 2015. Cement sheath integrity during thermal cycling: A novel approach for experimental tests of cement systems. SPE Bergen one Day Seminar. OnePetro. https://doi.org/10.2118/173871-MS.

Dugonjic-Bilic, F., Tiemeyer, C., Plank, J., 2011. Study on admixtures for calcium aluminate phosphate cement useful to seal CCS wells. In: SPE International Symposium on Oilfield Chemistry. OnePetro. https://doi.org/10.2118/141179-MS.

Eiken, O., Ringrose, P., Hermanrud, C., Nazarian, B., Torp, T.A., Høier, L., 2011. Lessons learned from 14 years of CCS operations: Sleipner, In Salah and Snøhvit. Energy Procedia 4, 5541–5548. https://doi.org/10.1016/j.egypro.2011.02.541.

Haszeldine, R.S., 2009. Carbon capture and storage: How green can black be? Science 325 (5948), 1647–1652. https://doi.org/10.1126/science.1172246.

Kirby, G.A., Chadwick, R.A., Holloway, S., 2001. Depth Mapping and Characterisation of the Utsira Sand Saline Aquifer, Central and Northern North Sea. *British Geological Survey Report* CR/01/218N. British Geological Survey.

Kvassnes, A., & Clausen, J.A. (.2020). U.S. Patent No. 10,774,001. Washington, DC: U.S. Patent and Trademark Office.

Kvassnes, A., & Clausen, J.A. (.2021). U.S. Patent No. 11,014,851. Washington, DC: U.S. Patent and Trademark Office.

Lescanne, M., Hy-Billiot, J., Aimard, N., Prinet, C., 2011. The site monitoring of the Lacq industrial CCS reference project. Energy Procedia 4, 3518–3525. https://doi.org/10.1016/j.egypro.2011.02.279.

Lesti, M., Tiemeyer, C., Plank, J., 2013. CO_2 stability of Portland cement based well cementing systems for use on carbon capture & storage (CCS) wells. Cem. Concr. Res. 45, 45–54. https://doi.org/10.1016/j.cemconres.2012.12.001.

Lund, H., Torsæter, M., Munkejord, S.T., 2015. Study of thermal variations in wells during CO_2 injection. SPE Bergen One Day Seminar. OnePetro. https://doi.org/10.2118/173864-MS.

Metz, B., Davidson, O., De Coninck, H.C., Loos, M., Meyer, L., 2005. IPCC Special Report On Carbon Dioxide Capture and Storage. Cambridge University Press, Cambridge.

Neville, A.M., Brooks, J.J., 1987. Concrete Technology, 438. Longman Scientific & Technical, England.

Parker, M.E., Meyer, J.P., Meadows, S.R., 2009. Carbon dioxide enhanced oil recovery injection operations technologies. Energy Procedia 1 (1), 3141–3148. https://doi.org/10.1016/j.egypro.2009.02.096.

Roy, P., Walsh, S.D., Morris, J.P., Iyer, J., Hao, Y., Carroll, S., Torsæter, M., 2016. Studying the impact of thermal cycling on wellbore integrity during CO_2 injection. In: 50th US Rock Mechanics/Geomechanics Symposium. OnePetro.

Samara, H., Al-Eryani, M., Jaeger, P., 2022. The role of supercritical carbon dioxide in modifying the phase and interfacial properties of multiphase systems relevant to combined EOR-CCS. Fuel 323, 124271. https://doi.org/10.1016/j.fuel.2022.124271.

Santra, A., Sweatman, R., 2011. Understanding the long-term chemical and mechanical integrity of cement in a CCS environment. Energy Procedia 4, 5243–5250. https://doi.org/10.1016/j.egypro.2011.02.503.

Selma, L., Seigo, O., Dohle, S., Siegrist, M., 2014. Public perception of carbon capture and storage (CCS): a review. Renewable Sustainable Energy Rev. 38, 848–863. https://doi.org/10.1016/j.rser.2014.07.017.

Son, H.M., Park, S.M., Jang, J.G., Lee, H.K., 2018. Effect of nano-silica on hydration and conversion of calcium aluminate cement. Constr. Build. Mater. 169, 819–825. https://doi.org/10.1016/j.conbuildmat.2018.03.011.

Torsæter, M., Todorovic, J., Lavrov, A., Gawel, K., Lund, H., Roy, P., Carroll, S., 2017. Avoiding damage of CO_2 injection wells caused by temperature variations. Energy Procedia 114, 5275–5286. https://doi.org/10.1016/j.egypro.2017.03.1645.

Vilarrasa, V., Rutqvist, J., 2017. Thermal effects on geologic carbon storage. Earth Sci. Rev. 165, 245–256. https://doi.org/10.1016/j.earscirev.2016.12.011.

Yoo, B.Y., Choi, D.K., Kim, H.J., Moon, Y.S., Na, H.S., Lee, S.G., 2013. Development of CO_2 terminal and CO_2 carrier for future commercialized CCS market. Int. J. Greenhouse Gas Control 12, 323–332. https://doi.org/10.1016/j.ijggc.2012.11.008.

Zhang, K., Lau, H.C., Chen, Z., 2022. Extension of CO_2 storage life in the Sleipner CCS project by reservoir pressure management. J. Nat. Gas Sci. Eng. 108, 104814 https://doi.org/10.1016/j.jngse.2022.104814.